

FLUID-STRUCTURE INTERACTION (FSI) MODELING OF THIN PLATES

C.J. Jesse, J.C. Kennedy and G.L. Solbrekken

Department of Mechanical and Aerospace Engineering, University of Missouri

Lafferre Hall, Columbia, MO 65211, USA

cj8q5@mail.missouri.edu, jckx84@mail.missouri.edu, solbrekkeng@missouri.edu

ABSTRACT

The fluid-structure interaction (FSI) of both flat and curved plates in parallel flow has been successfully simulated using popular numeric codes. The FSI models are carried out using a prototypic geometry of one 1.016 mm (40 mils) plate bounded by fluid channels of differing thickness. The modeled plate uses isotropic structural properties of Al 6061-T6 while the fluid is assumed to be water. High velocity flow combined with the dissimilar fluid channel gaps leads to a pressure differential across the plate that causes plate deflection. The plate's structural behavior is modeled using Abaqus, a finite element based code, and the fluid flow in the channels is modeled using Star-CCM+, a control volume based code.

A loosely coupled (explicit) scheme is utilized in the FSI models in an effort to decrease runtime. However, utilizing a loosely coupled scheme amplifies solution-destabilizing behavior of the FSI models for the complex problem evaluated. In particular, incompressible turbulent flow around a slender geometry and comparable densities of the fluid and the structure contribute to solution instability. The iterative data exchange between the computational domains therefore needs to be managed very carefully depending on the spatial mesh used and the time step employed in the models.

It was discovered that the range of stable time steps diminishes with increasing flow velocity. Furthermore, both an upper and lower limit of stable time steps was found through a range of flow velocities. These upper and lower limits on the time step are likely dependent on the spatial mesh used.

The flat plate FSI models were compared to both curved plate models and experiment data collected using the Hydro-Mechanical Flow Loop at the University of Missouri. It was found that the curved plate models deflected less than the flat plate models by more than an order of magnitude. This is due to the increased stiffness of the curved plates. Comparison to the experiment shows the flat plate models deviating from the experiment data. It is hypothesized this is a result of assuming idealized geometry in the models when in reality the experiment has small geometric deviations. Thus, future FSI models should account for these geometric deviations in the experiment to help facilitate convergence of the experimental data with the model's predicted solutions.

KEYWORDS

Fluid-Structure Interaction (FSI), Finite Element Method (FEM), Computational Fluid Dynamics (CFD), Code-Coupling

1. INTRODUCTION

In 2004, the National Nuclear Security Administration (NNSA) merged the Reduced Enrichment for Research Test and Reactors (RERTR) program with other non-proliferation programs to form the Global Threat Reduction Initiative (GTRI). One of the primary objectives of the GTRI is to convert the five U.S. high-performance research reactors (HPRR), including the University of Missouri Research Reactor (MURR), from high enriched uranium (HEU) fuel to low enriched uranium (LEU) fuel. The GTRI program is currently investigating a novel monolithic LEU fuel that utilizes a U-Mo alloy fuel [1]. For the

proposed LEU fuel to be fully qualified for in-reactor use, the design needs to be studied from a hydro-mechanical perspective.

The HPRRs were designed with unique plate type fuels to promote performance however; they may be susceptible to hydro-mechanical instabilities due to their tall and thin nature. To predict if these instabilities might occur during in-reactor use, fluid-structure interaction (FSI) models were built by explicitly coupling Star-CCM+, a control volume based code, and Abaqus, a finite element based code [2, 3]. Both flat and more prototypic curved plates were modeled. For validation purposes, the flat plate models were compared to experiments completed using the Hydro-Mechanical Flow Loop (HMFL) at the University of Missouri [4]. They were then compared to the curved plate models to reveal the influence of curvature.

1.1. Previous Theoretical and Experimental Studies

The hydro-mechanical stability of plate type fuels has been of interests since at least the 1950s. However, understanding the stability of plates under high velocity flows is difficult since it requires solving fluid dynamics and solid mechanics problem simultaneously. In 1958, Miller developed analytic models for the deflection of simple plate geometries when subjected to a cross-plate pressure differential caused by a coolant flow imbalance [5]. His derivations coupled wide beam theory with the cross-plate coolant pressure difference using Bernoulli's equation to derive critical velocity formulas. For a single flat plate with two flow channels the critical velocity formula is

$$V_{c,1} = \left(\frac{30Ea^3h}{\rho_f d^4 (1 - \nu^2)} \right)^{1/2} \quad (1)$$

where E , ν , a , and d are the Young's modulus, Poisson's ratio, plate thickness, and width of the plate and ρ_f and h are the density and fluid channel thickness. While Miller's critical velocity equations provide utility in defining a boundary between stable and unstable flow conditions, it does lack significant features like accounting for differing channel thicknesses.

Miller's paper prompted many researchers to complete experimental studies. In 1958 and 1959, Zabriskie completed hydro-mechanical experiments in an effort to validate Miller's models [6]. He found that the critical velocity described a point of large deflection rather than a full plate collapse. Groninger et al. and Smissaert also arrived at similar conclusions about the critical velocity [7, 8].

1.2. Difficulties of Numerically Modeling Fluid-Structure Interaction (FSI)

Up until recently, utilizing analytic and experimental techniques have been the only methods to quantify the significance of fluid-structure interaction in HPRR plate-type fuels. Initially numeric FSI modeling was developed in the aerospace industry to describe how an elastically deforming aircraft wing responds within an in-flight flow field [9]. These models were coupled using *partitioned* methods where the fluid and solid domains are solved independently and iteratively exchange data at the fluid-structure boundary. This has become a popular approach because numerous methods and commercial codes exist in these respective domains. Furthermore, the existing codes and methods are considered state of the art, and thus known to provide excellent results in their individual domains. Therefore, when coupled they should maintain their efficiency and accuracy; however, this is not always true under certain physical and numeric conditions.

When a *partitioned* method iterates the fluid and solid domains only once per time step it is known as a loose (explicit) coupling scheme. In contrast strongly (semi-implicit) coupled schemes iterate multiple

times within a time step. Loose coupling is advantageous from a computational efficiency standpoint, but unfortunately, outside of aeroelastic problems, loose coupling is only conditionally stable. Instabilities most frequently occur when the densities of the fluid and the structure are similar and/or when the geometry is slender [10, 11]. These instabilities are amplified when the flow is incompressible. The incompressibility of the fluid causes it to act as an additional mass on the structure and causes instability. The instability is so severe and prominent that it has been named the “added-mass effect”. It has also been shown to enforce a lower bound on the range of stable time increments for conditionally stable FSI models that utilize loose coupling schemes [11].

2. NUMERIC MODELS

2.1. Fluid Model

The geometry of the parallel plate assembly explored in this paper included a thin flat aluminum plate within a slender flow channel. A generic diagram of this geometry is shown in Figure 1.

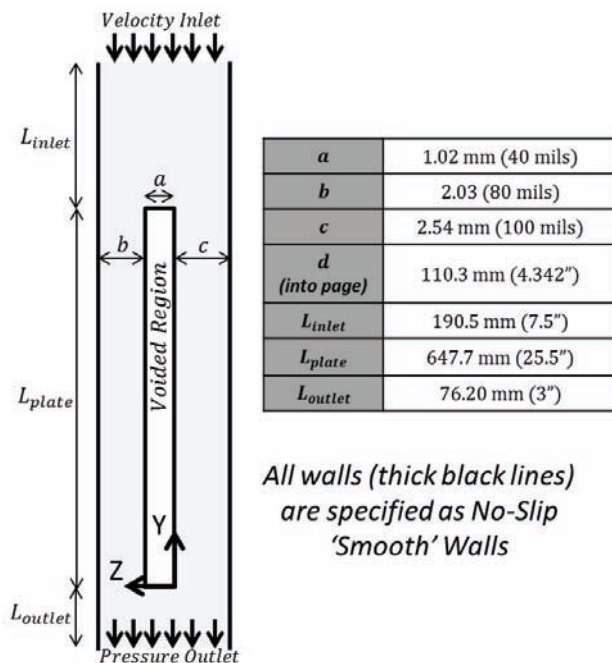


Figure 1. Fluid model geometry with dimensions (not to scale).

The fluid flow around the “voided region” (where the plate resides) was water with a density of 997.6 kg/m^3 and a dynamic viscosity of $0.8871 \text{ mPa}\cdot\text{s}$. Overall, this geometry’s dimensions were based on the nominal dimensions from the experiment [4]. The 1.016 mm (40 mils) thick plate was purposely offset within the flow channel for two reasons: First, the offset simulated the effect of assembly tolerances. Second, it drove the FSI problem by creating a flow imbalance within the fluid channels, which caused the plate to deflect. For all FSI models the plate was offset by 0.254 mm (10 mils) causing the fluid channels to be 2.032 mm (80 mils) and 2.540 mm (100 mils) thick. Overall, the computational domain was 5.588 mm (220 mils) thick and 914.4 mm (36") long. This created a very slender high-aspect ratio geometry of 164:1. The inlet of the model was assumed a uniform velocity inlet, the outlet was assumed a 0 Pa pressure outlet, and all the walls were assumed “smooth” with no slip.

The water flow around the flat plate in Figure 1 was simulated using the commercial CFD code Star-CCM+ [2]. The fluid mesh at the leading and trailing edge of the plate is shown in Figure 2A. This mesh contains about 900,000 cells. The flow in the CFD model was assumed an incompressible turbulent flow. To estimate the solution of the turbulent flow a Reynold’s Averaged Navier Stokes (RANS) model was utilized. After comparing a suite of RANS models to a simple 1D analytic model with a rigid plate, the Realizable $k-\epsilon$ Two Layer All y^+ model was found to match the best (using the fluid mesh in Figure 2) with $< 0.5\%$ error from the analytic model. The All y^+ wall treatment has the ability to emulate the high y^+ treatment when wall cells have y^+ values within the log-law region of the boundary layer ($y^+ \geq 30$) and the low y^+ wall treatment when wall y^+ values are ~ 1 . It can also produce acceptable solutions when wall cells are within the buffer region of the boundary layer. Therefore, the All y^+ wall treatment is a good fit for this fluid model since the mesh will be morphing around the deforming plate when its utilized

in an FSI model, which will cause the wall y^+ values to fluctuate. Finally, the numerical solvers are second-order accurate in space and first-order accurate in time in an effort to increase stability [11].

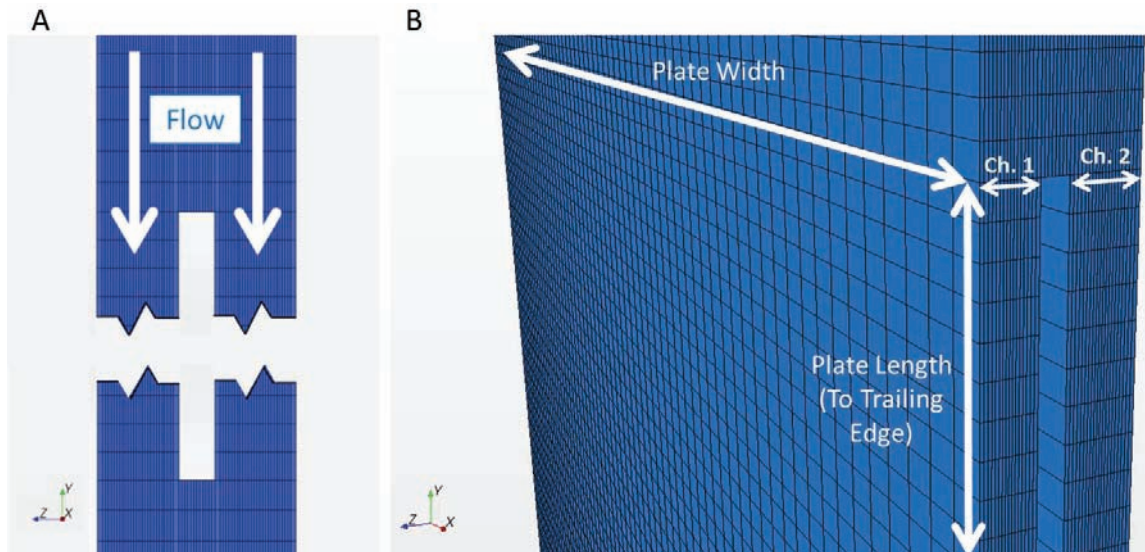


Figure 2. Fluid mesh in Star-CCM+.

1.1. Plate Model

The deformation of the flat plate was modeled using the commercial FEM code Abaqus [3]. The plate geometry and mesh in Abaqus are shown in Figure 3. An extra 0.5" was added to both sides of the plate to mimic how the experiment clamps the plate. These surfaces (shaded red in the figure) were restricted from moving in the X, Y, and Z directions. Since both the front and back of the plate were pinned, rotation was also restricted. The mesh in Figure 3B contains about 160,000 elements and it was created with C3D8I elements.

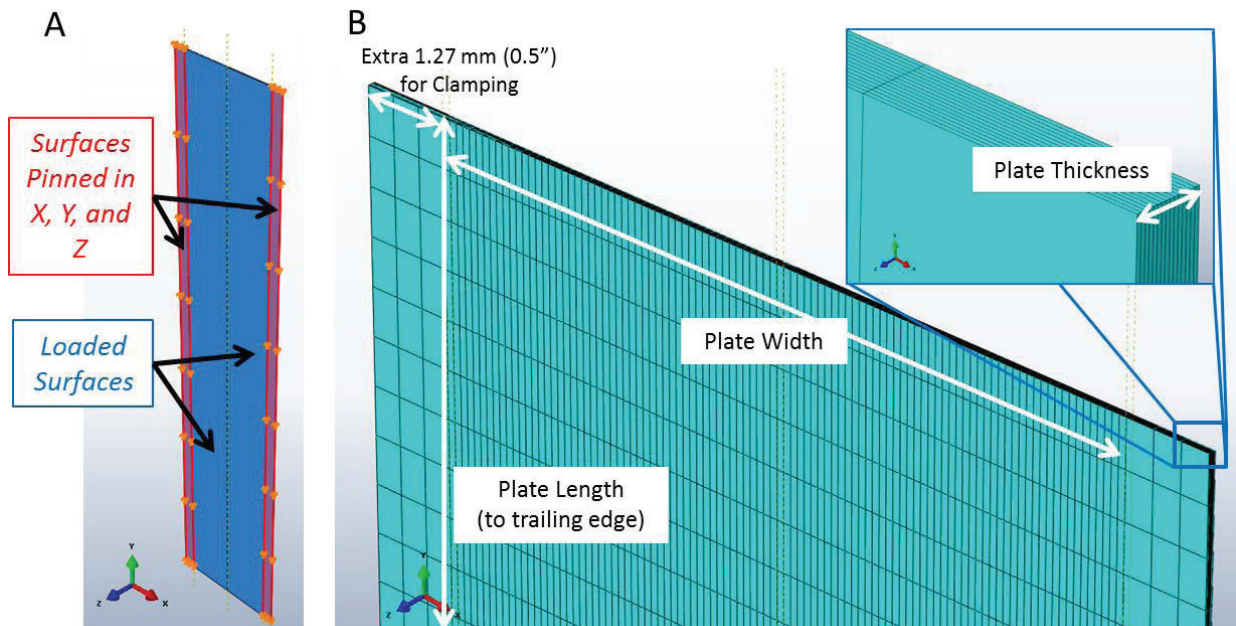


Figure 3. Plate model (A) and mesh (B) in Abaqus.

The plate was modeled as Al-6061-T6 with a Young's modulus of 68.9 GPa, a Poisson's ratio of 0.33, and a mass density of 2700 kg/m³. Finally, the Abaqus option "Nlgeom" was turned on to assure 3D effects that occur during plate bending will be included.

1.2. Coupling the Fluid and Plate Models

The capability to couple Abaqus and Star-CCM+ using a loose coupling scheme, called explicit coupling by CD-Adapco, is built-in to the codes. This explicit coupling process is outlined in Figure 4A.

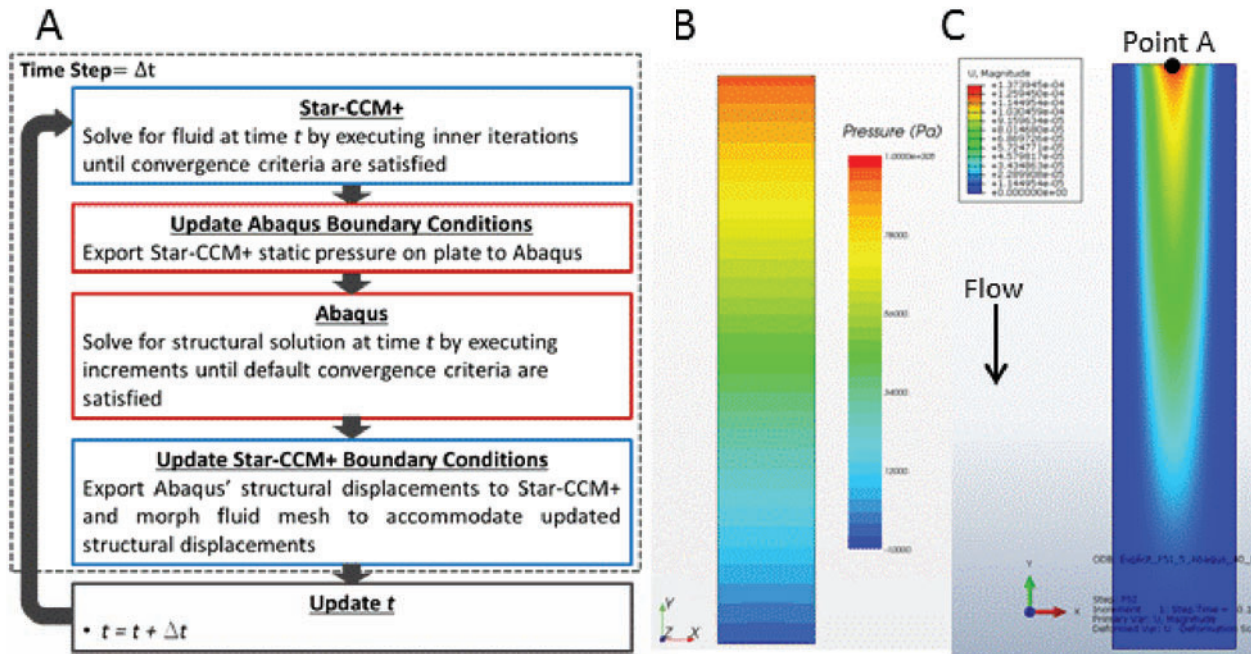


Figure 4. Abaqus and Star-CCM+ explicit coupling process with converged pressure/deflection solutions in Abaqus and Star-CCM+.

At the beginning of an FSI model Star-CCM+ iterates the pressure/flow fields until the pressure and wall shear stress values on the surface of the plate each change by less than 1 Pa for 25 consecutive iterations. Figure 4B shows an example of the pressure distribution on the surface of a perfectly flat plate (fluid/structure interface) in Star-CCM+. This static pressure field is then exported to the surface of the plate (fluid/structure interface) in Abaqus. Using this pressure field from Star-CCM+, Abaqus iterates until Abaqus' default convergence criteria are satisfied yielding a plate deformation similar to Figure 4C. This plate deformation is then exported to Star-CCM+ and the mesh is morphed using Star-CCM+'s built-in mesh morpher. Morphing the mesh allows flow redistribution to be simulated around the newly deformed plate. In this staggered approach, the FSI model assumes convergence at the fluid/structure interface and moves forward in time. Thus, at the next time step Star-CCM+ will be simulating flow redistribution around a plate with a deformation solution from the previous time step, which will create a portion of artificial fluid forces at the fluid/structure interface, i.e. coupling forces. Fortunately, these artificial coupling forces will not decrease the accuracy of a model that avoids instability and successfully reaches a steady state; however, these artificial forces may lead to a runaway buildup of excess energy at the fluid-structure interface and cause the model to go unstable before it can reach a steady state. Nonetheless, the process in Figure 4A is repeated until the model converges to a steady state or until it diverges.

Previously, FSI models, with nearly the same geometry shown in Figure 1 were completed by explicitly coupling Abaqus and Star-CCM+ [12]. To promote stability, a flow ramping technique was utilized where the inlet velocity was gradually increased. The technique proved successful, but runtimes were approximately a month due to using a ~22 million cell mesh, which was necessary to maintain stability. For the models in this paper, it was desired to keep the runtimes down to about a day while maintaining stability at flow velocities around 8 m/s. It should be noted from this point on; the term “converged” will indicate an FSI model has advanced to a steady-state plate deflection.

FSI models were attempted at flow velocities ranging from 2 to 8.25 m/s, however instead of gradually increasing the flow velocity within one FSI model; it was fixed in a suite of models. For example, once an FSI model at a velocity of 3 m/s converged, a new model was built at a flow velocity of 3.5 m/s. If an FSI model did not converge at a specific velocity, the model was rerun using a smaller time step to increase stability as suggested in literature [10]. The flow velocity was incrementally increased in ~0.5 m/s increments until decreasing the time step did not increase stability enough to allow the FSI model to converge. Finally, a large parametric study was completed by varying the time step at a variety of velocities ranging from 2 to 8.25 m/s to reveal how the time step affects stability.

3. CODE COUPLING RESULTS

3.1. Velocity Sweep

Converged FSI models were attained at flow velocities ranging from 2 to 8 m/s. Figure 5 shows how the deflection at “Point A” on Figure 4C (the location of maximum deflection) behaved as the velocity was increased. The plot includes a power law curve fit that suggests the deflection increases with nearly the square of flow velocity. At higher flow velocities, the deflection trend increased more rapidly. While second order behavior with velocity is consistent with linear drag analysis, non-linear behavior is an indicator of structural changes in the system. Deflection contour plots in Abaqus can provide some guidance as to what may be happening.

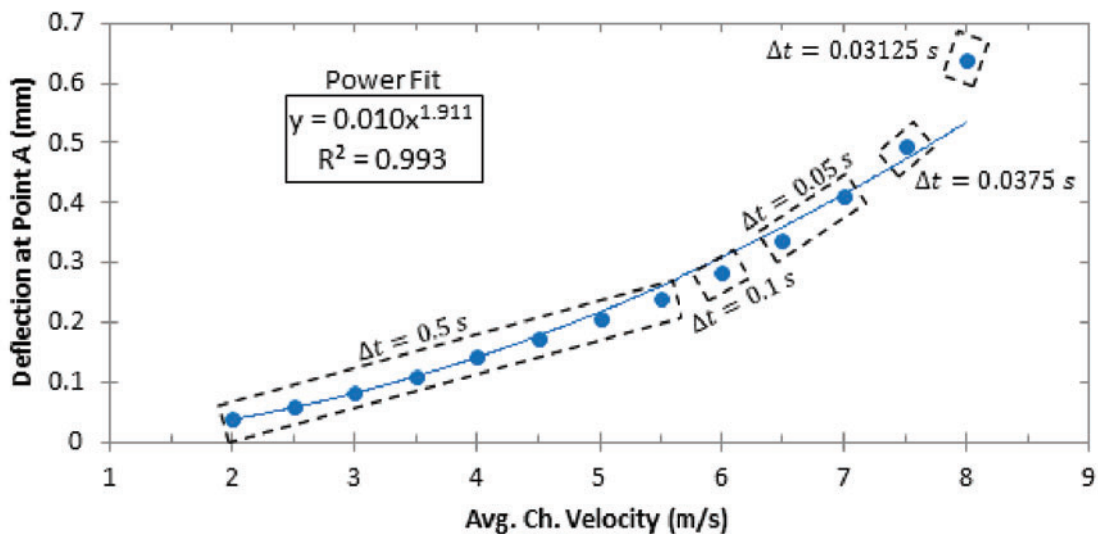


Figure 5. Deflection at Point A vs. velocity with the time step utilized at each velocity.

The deflection contours from Abaqus at 5 m/s and 8 m/s are shown on the left and right of Figure 6. At 5 m/s, the model predicts one deflection peak at the leading edge whereas at 8 m/s the model predicts three distinct peaks; the first at the leading edge, the second at about halfway from the leading edge, and the

third towards the trailing edge of the plate. The difference in these two plate deformations likely explains why the curve fit begins deviating from the data at ~ 5.5 m/s in Figure 5.

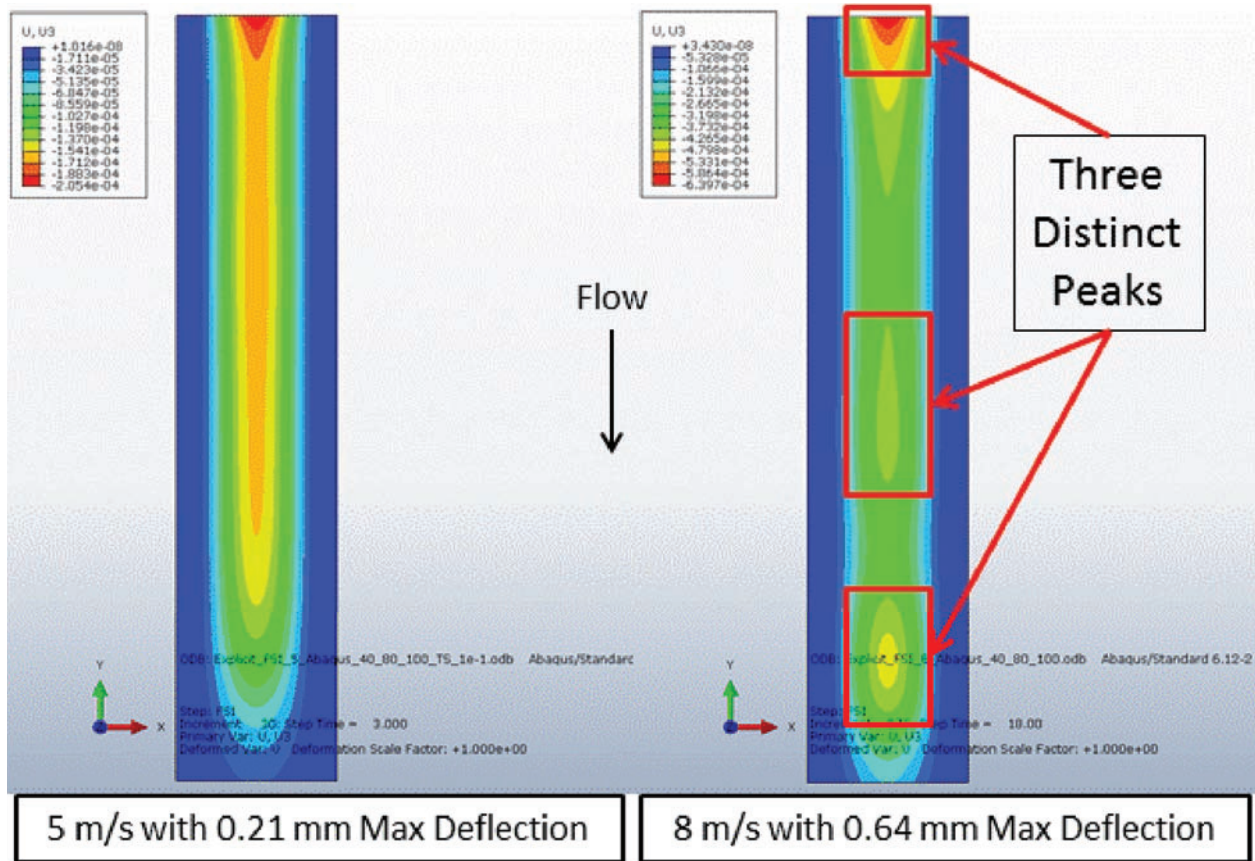


Figure 6. Contours of deflection at 5 and 8 m/s, flow moves down in the $-Y$ direction.

3.2. Time Step Parametric Study

The map in Figure 7 shows how varying the time step at a particular velocity affects stability. Three regions are highlighted on the map: First, the green region, which indicates time steps that allowed the model to converge. Second, the yellow region, which indicates time steps that allowed the models to converge to steady-state deflections significantly higher from those in the green region and/or they converged to a stable plate oscillation. Finally, the red region, which indicates time steps that caused the models to diverge and/or crash. The range of stable time steps begins to narrow rather quickly as the velocity increases beyond 5.25 m/s. Interestingly, this is where the deflection profile of the plate begins to vary. Furthermore, the Miller Critical velocity (6.14 m/s) also lies within this band of rapidly decreasing stable time steps. It should be noted that while Miller's critical velocity does not directly apply to these models (due to uneven fluid channels) it was estimated assuming equal channel thicknesses of 2.286 mm (90 mils). At velocities around 7.5 and 8 m/s the range of stable time steps is small and it appears to be nonexistent at velocities > 8 m/s.

Figure 8 illustrates how the evolution of the FSI model changes within the four regions of Figure 7. The color of the curves corresponds to the red, green, and yellow regions in Figure 7. The zoomed in view shows the green curve, the $\Delta t = 0.05$ s response, converging to a steady state. Conversely, the dotted red curve, the $\Delta t = 5$ s response, shows the model oscillating between the two flow channels, hence, the positive (deflection into the 2.54 mm (100 mils)) and negative (deflection into the 2.03 mm (80 mils))

values. This caused the model to crash due to a floating-point exception (FPE) in the turbulence model. The FPE was a result of the cells through the thickness of the fluid channels becoming very thin. Similarly, the dashed red curve, the $\Delta t = 0.03$ s response, shows oscillations between the channels. The large magnitude of deflection caused the cells through the thickness of the channel to crush triggering negative cell volume errors. The yellow curve, the $\Delta t = 0.03$ s response, also shows oscillatory behavior. However, the oscillation stayed within the 2.54 mm (100 mils) channel and converged to a steady-state oscillation with slightly higher deflection than the $\Delta t = 0.05$ s response.

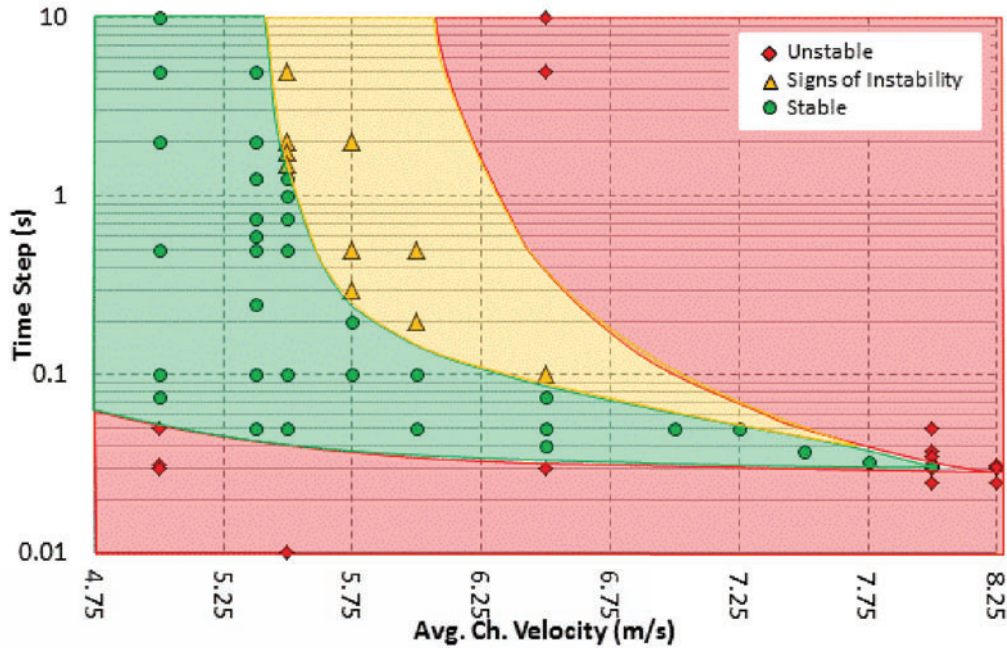


Figure 7. Map of stable, mildly unstable, and unstable time steps from 4.75 to 8.25 m/s.

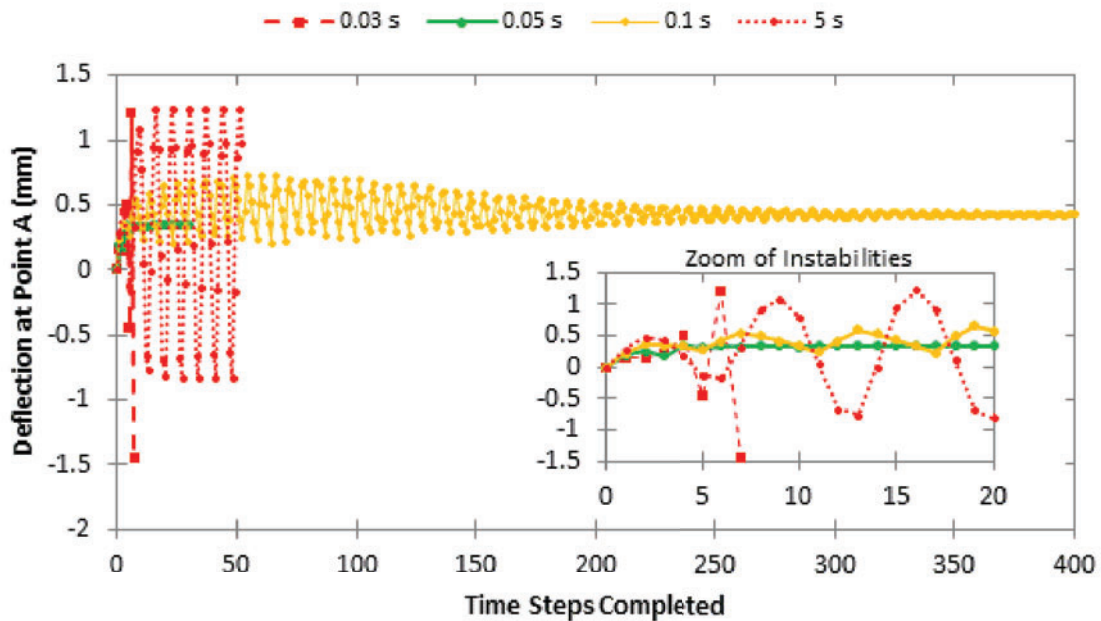


Figure 8. Evolution of plate deflection at Point A with various time steps at 6.5 m/s.

There appears to be both a lower and upper limit of stable time increments. The explicit nature of the coupling algorithm likely creates a CFL condition, which is possibly the cause of the upper bound seen in Figure 7. Forester et al. theoretically showed that stabilized FSI models might become unstable with small time steps when utilizing loose coupling schemes [11]. The instability was traced back to the inherent added-mass effect of incompressible flows. Therefore, the added-mass effect in these models is likely causing the lower bound on the time step seen in Figure 7.

4. COMPARISON TO FLOW EXPERIMENTS

Hydro-mechanical experiments at the University of Missouri have been completed using the Hydro-Mechanical Flow Loop [4] to provide experimental validation of the solutions predicted in the FSI models. A diagram of the test section utilized in the experiment is shown in Figure 9.

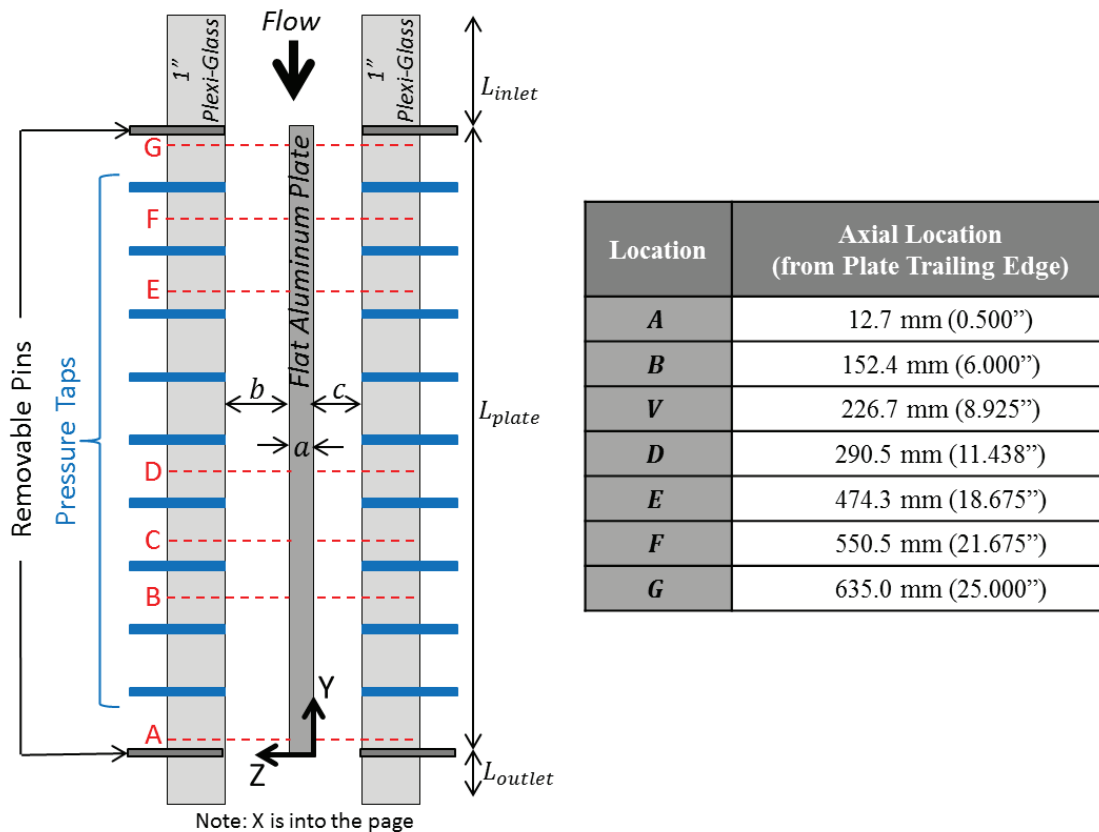


Figure 9. Diagram of experiment test section with deflection measurement locations.

This geometry is ideally identical to the geometry and dimensions in Figure 1. The seven dashed red horizontal lines show where laser displacement sensors were placed to measure the change in the thickness of the channel gap, i.e. plate deflection, as the flow deforms the Al 6061-T6 plate. One laser sensor, “Laser A”, observed the 2.54 mm (100 mils) channel while the other laser sensor, “Laser B”, observed the 2.03 mm (80 mils) channel. It should be noted before water was driven through the test section the laser sensors were utilized to map the initial thickness of the channel gaps at 120 XY locations (12 points in the X direction and 10 points in the Y direction). This data helps explain why the plate deflects in unexpected ways when water is forced through the test section.

To compare the FSI models to the experiment data the change in channel gap measurements from both lasers were compared to the axial centerline deflection profiles from the FSI models. It should be noted, the experimental measurements for a given flow velocity were collected at different points in time such that they cannot conclusively be interpreted as the axial profile of the plate for that flow velocity. The experiment velocity in each of the subsequent comparison plots are averages of the measured velocities when each individual channel gap measurement was taken. Experiment data are plotted as red diamonds (Laser A) and yellow points (Laser B) while solutions from the models are plotted as blue and green lines. From this point on “large channel” will refer to the 2.54 mm (100 mils) channel and “small channel” will refer to the 2.03 mm (80 mils) channel.

The first comparison, shown in Figure 10, is at ~ 2 m/s. Nearly all the data points from the experiment show the plate deflecting into the small channel. This is counter to all the FSI models, which exclusively predicted all deflection to be into the large channel. However, if this fact is ignored, qualitatively the trend from “Laser B” near the leading and trailing edges follows the models for the most part. Furthermore, through the mid-section of the plate, from ~ 0.3 to ~ 0.5 m, “Laser B” shows the plate “bulging” into the small channel, which never appears in the models.

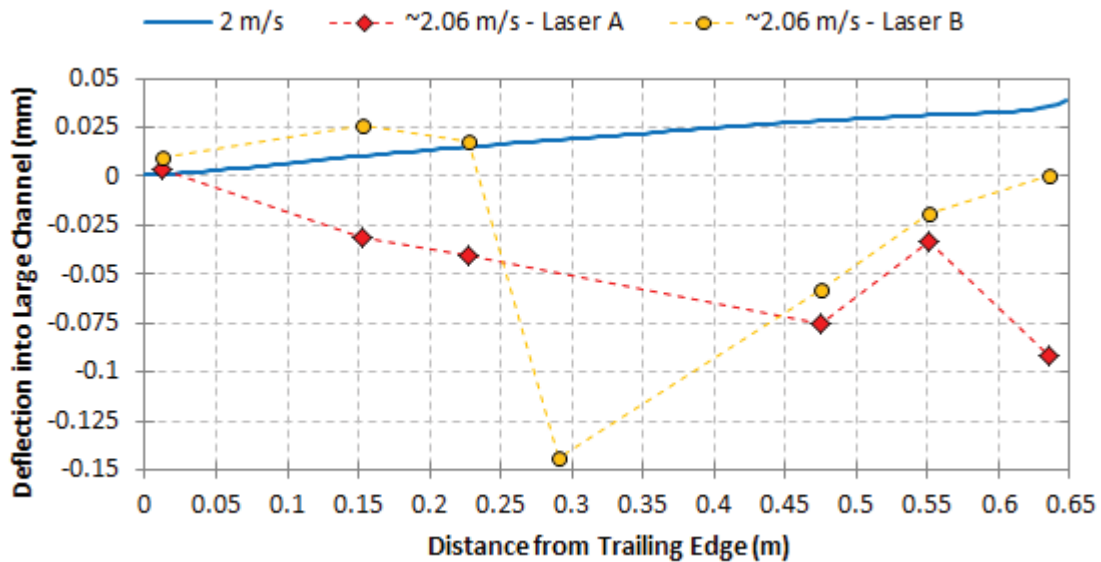


Figure 10. Comparison to the model (solid line) to the experiment at ~ 2.06 m/s.

The next comparison, shown in Figure 11, is at ~ 5 m/s. In contrast to the comparison at ~ 2 m/s, the experiment shows deflection almost entirely into the large channel. It appears that as the flow velocity is increased in the experiment the plate begins moving from the small channel to the large channel. This comparison matches better than the previous comparison, but overall it appears the model is incorrectly predicting the shape of the deformed plate.

In Figure 12 the experiment shows the plate deflecting completely into the small channel at ~ 7.75 m/s. The magnitude of the deflection from the experiment is more than double the deflection predicted by the model. This unexpected behavior is in contrast to all the FSI models and is a strong indicator that additional features from the experiment need to be added to the models for more accurate predictions.

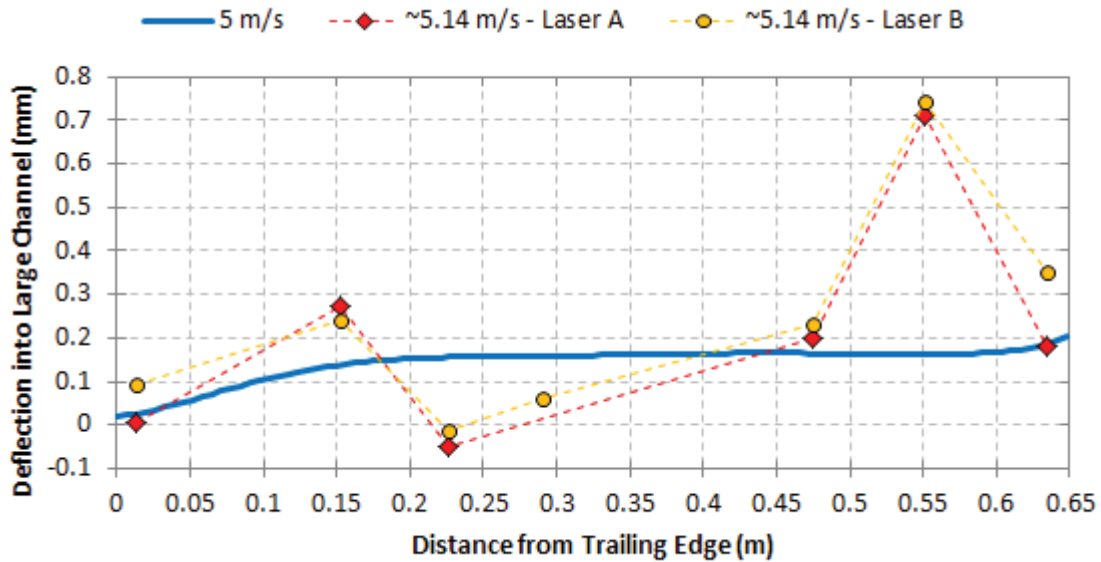


Figure 11. Comparison to the model (solid line) to the experiment at ~5.14 m/s.

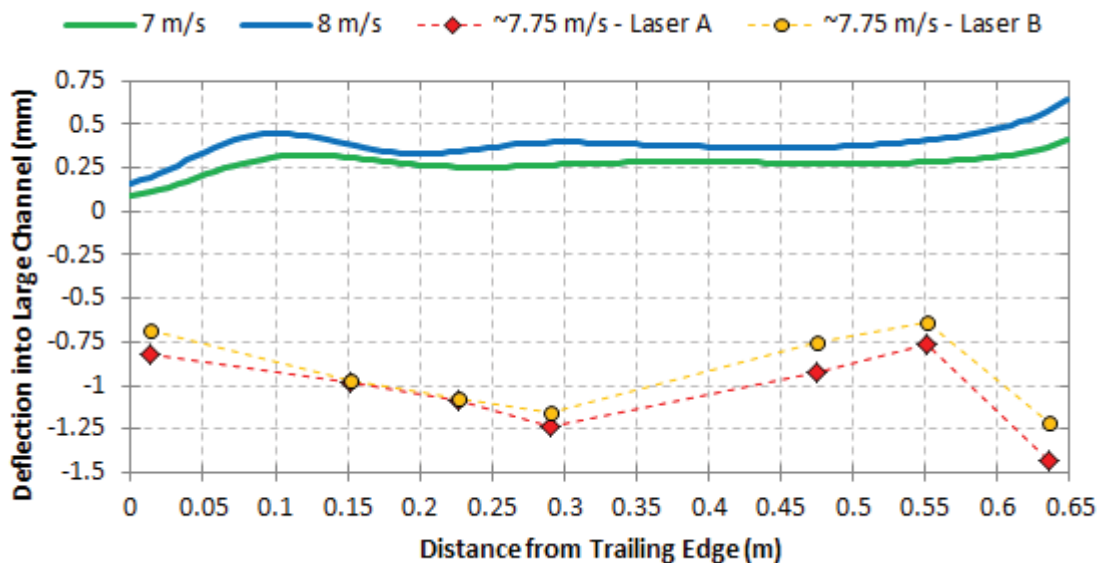


Figure 12. Comparison of the models (solid lines) and the experiment at ~7.75 m/s.

A possible explanation for the atypical behavior seen in the experiment can be revealed by examining the initial (no flow) geometry of the flow channels. As mentioned earlier the thicknesses of the channel gaps were measured before water was forced through the test section. These initial channel gap thicknesses (measured before the flow experiments) were used to calculate the differential in the thickness of the large and small channels. The red points in Figure 13 show these differentials at approximately the axial centerline of the plate. It is apparent that the initial channel difference assumed in the models differs significantly from the values measured in the experiment. Thus, it is likely that the dissimilarities between the models and the experiments in Figure 10-12 is a result of the drastic variance between the geometry assumed in the models and the actual geometry measured in the experiments.

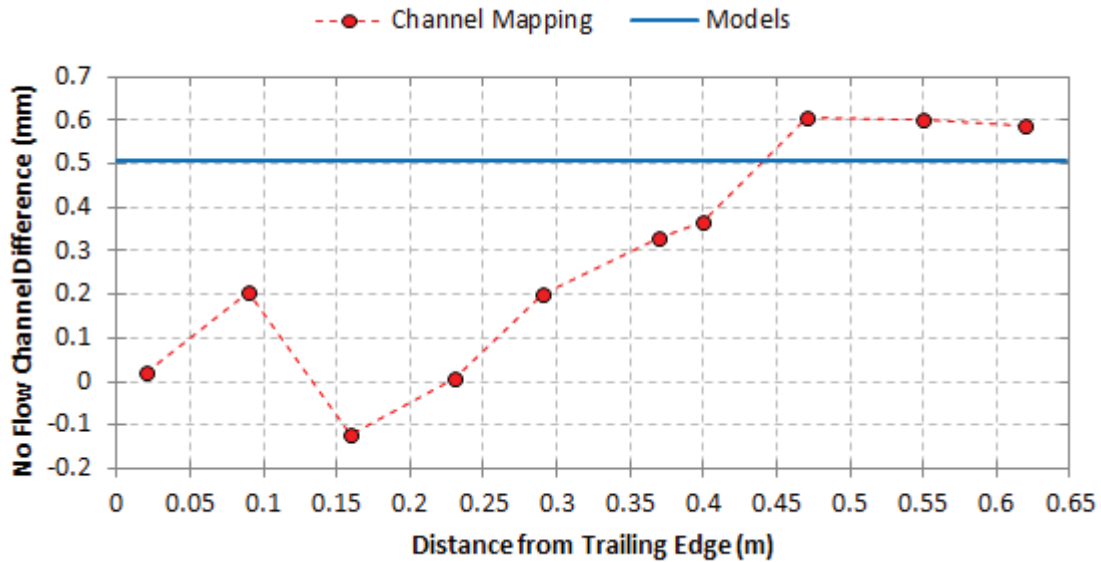


Figure 13. Comparison of the channel difference assumed in the models and measured during the channel mapping.

5. PROTOTYPIC CURVED PLATE MODELING

Flat plates have been utilized in all the FSI models and experiments presented thus far, however the MURR fuel elements contain curved fuel plates as shown in Figure 14.

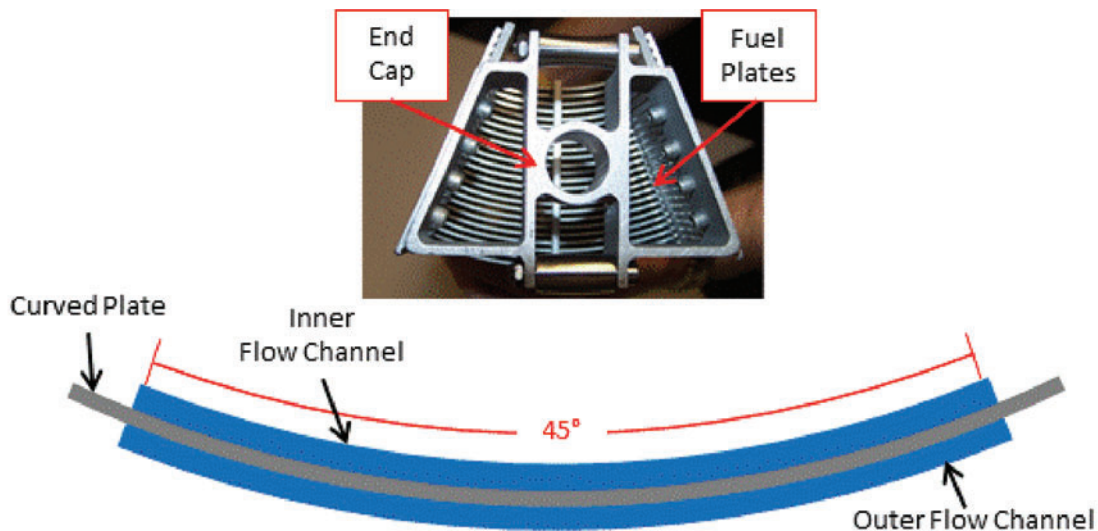


Figure 14. Curved plate geometry with photo of mock MURR fuel element.

The plates in the MURR fuel elements are nested within a $\sim 45^\circ$ arc. The curved plate FSI models were built to mimic this configuration by nesting a single 0.9652 mm (38 mils) plate within a 45° arc that was 110.3 mm (4.342") long. The thickness of the flow channel on the inner radius was 2.032 mm (80 mils) and the thickness of the flow channel on the outer radius was 2.540 mm (100 mils). All other dimensions were identical to the flat plate models. The curved plate models were completed from 3 to 8 m/s using a time step of 0.05 s. It was found that the curved plate models were considerably more stable than the flat

plate models at similar velocities. This is likely because the curved plate models deflected significantly less than the flat plate models.

To understand how plate curvature affects hydro-mechanical deflection of thin plates the previously discussed flat plate models were compared to the curved plate models. Table I compares the maximum leading edge deflection from the flat and curved plate models. The maximum deflection occurred at Point A (Figure 4C) in all models and deflections were always into the large channel. It is apparent that the curved plates are about two orders of magnitude stiffer than the flat plates. Interestingly, the % difference at 7 and 8 m/s is appreciably higher than at lower velocities. This is likely because the overall shape of the deformed flat plates begins to significantly differ around 7-8 m/s (Figure 6).

Table I. Comparing the maximum deflection of flat and curved plates.

Velocity (m/s)	Deflection at Point A (mm)		% Difference
	1.02 mm (40 mils) Flat Plate	0.97 mm (38 mils) Curved Plate	
3	0.0833	0.0010	7866%
4	0.1417	0.0017	8336%
5	0.2053	0.0025	8261%
6	0.2837	0.0034	8345%
7	0.4112	0.0043	9482%
8	0.6397	0.0048	13133%

6. CONCLUSIONS

The FSI modeling of flat plates has been successfully accomplished through explicitly coupling the commercial codes Star-CCM+ and Abaqus. Keeping the FSI models stable was difficult due to the difficulty of coupling an incompressible flow with a slender structure, often called the “added-mass effect”. It was found that both an upper and lower bound on stable time steps exists. The upper bound is likely a result of CFL condition due to the explicit nature of the coupling and the lower bound likely appears due to the added-mass effect that appears when incompressible flows are explicitly coupled with slender structures. The upper and lower bounds on stable time steps are likely dependent on the spatial meshes used as well as other parameters in the FSI models.

The stabilized flat plate FSI models were then compared to experiments conducted with the HMFL at the University of Missouri. It was found that the predicted solutions from the models largely differed from the data measured in the flow experiments. The discrepancies were traced back to assuming in the models that the flow channels were uniformly thick when in reality the initial (no-flow) channel thicknesses measured before the flow experiments have numerous imperfections. Thus, it is highly suggested that future FSI models include these geometric imperfections by adjusting the locations of the fluid mesh nodes to mimic the geometry of the experiment more closely to facilitate the merging of the experimental data with the predicted solutions from the models.

FSI models with curved plates were simulated in order to understand a more prototypic MURR fuel plate. These curved plate models were then compared to the flat plate models to reveal the benefit of curvature. It was found that the curved plates decrease plate deflection by about two orders of magnitude. Furthermore, the fuel plates within the MURR fuel elements include a stabilizing comb at the leading and trailing edges, which will further decrease deflection. However, both the flat and curved plate models still need to be benchmarked against experiments. The full structure of the plate, including the different material layers, also needs to be evaluated. Once the FSI models are validated, they can be utilized to

model complicated geometries, such as a full MURR element, that are costly and/or difficult to investigate experimentally.

ACKNOWLEDGEMENTS

In addition to the University of Missouri, the authors would also like to thank John Stevens, Adrian Tentner, and Erik Wilson at Argonne National Laboratory for their support in this research. This work has been completed under Argonne National Lab (ANL) contract 6J-00005-0003A.

REFERENCES

- [1] D. Wachs, "Conceptual Process Description for the Manufacture of Low-Enriched Uranium-Molybdenum Fuel," Idaho National Laboratory, Idaho Falls, 2008.
- [2] CD-Adapco, *Star-CCM+ (Version 7.04.011 and 9.02.007-R8) [Software]*, 2014.
- [3] Simulia, *Abaqus CAE (Version 6.12-2 and 6.13-1) [Software]*, Simulia, 2013,2014.
- [4] J. C. Kennedy, C. J. Jesse, G. H. Schnieders and G. L. Solbrekken, "Experimental Investigation of Flat Plate Deflection Under Variable Velocity Parallel Flow," in *International Topical Meeting on Nuclear Reactor Thermal-Hydraulics (NURETH-16)*, Chicago, 2015.
- [5] D. R. Miller, "Critical Flow Velocities for Collapse of Reactor Parallel-Plate Fuel Assemblies," *ASME Journal of Engineering and Power*, pp. 83-91, 1960.
- [6] W. L. Zabriskie, "An Experimental Evaluation of the Critical Flow Velocity Formulas for Parallel Plate Assemblies," General Electric Co., Schenectady, N.Y., 1958.
- [7] R. D. Groninger and J. J. Kane, "Flow Induced Deflections of Parallel Flat Plates," *Nuclear Science and Engineering*, no. 16, pp. 218-226, 1963.
- [8] G. E. Smislaert, "Hydroelastic Instabilities in MTR-Type Fuel Elements," *Nuclear Engineering and Design*, no. 7, pp. 535-546, 1968.
- [9] C. A. Felippa, K. C. Park and C. Farhat, "Partitioned Analysis of Coupled Mechanical Systems," Department of Aerospace Engineering Studies and Center of Aerospace Structures University of Colorado Boulder, Boulder, CO, 1999.
- [10] P. Causin, J. F. Gerbeau and F. Nobile, "Added-mass effect in the design of partitioned algorithms for fluid-structure problems," *Computer Methods in Applied Mechanics and Engineering*, no. 194, pp. 4506-4527, 2005.
- [11] C. Forster, W. A. Wall and E. Ramm, "Artificial added mass instabilities in sequential staggered coupling of nonlinear structures and incompressible viscous flows," *Computer Methods in Applied Mechanics and Engineering*, no. 196, pp. 1278-1293, 2007.
- [12] J. C. Kennedy and G. L. Solbrekken, "Coupled Fluid Structure Interaction (FSI) Modeling of Parallel Plate Assemblies," in *ASME International Mechanical Engineering Congress & Exposition*, Denver, Colorado, 2011.